ACS APPLIED MATERIALS & INTERFACES

Research Article

www.acsami.org

Nucleation and Crystal Growth of Organic–Inorganic Lead Halide Perovskites under Different Relative Humidity

Hao Gao,[†,‡] Chunxiong Bao,[†] Faming Li,[†] Tao Yu,*[,†,§,∥] Jie Yang,[†] Weidong Zhu,[†] Xiaoxin Zhou,[†] Gao Fu,[†] and Zhigang Zou[†,§,∥]

[†]Department of Physics, National Laboratory of Solid State Microstructures & Ecomaterials and Renewable Energy Research Center (ERERC), Nanjing University, Nanjing 210093, P. R. China

[‡]School of Mechanical and Electronic Engineering, Jingdezhen Ceramic Institute, Jingdezhen 333001, P. R. China

[§]Collaborative Innovation Center of Advanced Microstructures, Nanjing University, Nanjing 210093, P. R. China

[∥]Jiangsu Key Laboratory for Nanotechnology, Nanjing University, Nanjing 210093, P. R. China

Supporting Information

ABSTRACT: Organic–inorganic lead halide perovskite compounds are very promising materials for high-efficiency perovskite solar cells. But how to fabricate high-quality perovksite films under controlled humidity conditions is still an important issue due to their sensitivity to moisture. In this study, we investigated the influence of ambient humidity on crystallization and surface morphology of one-step spin-coated perovskite films, as well as the performance of solar cells based on these perovskite films. On the basis of experimental analyses and thin film growth theory, we conclude that the influence of ambient humidity on nucleation at spin-coating stage is quite different from that on crystal growth at annealing stage. At the spin-coating stage, high nucleation density induced by high supersaturation prefers to appear under anhydrous circumstances, resulting in layer growth and high coverage of perovskite films. But at the annealing stage, the modest supersaturation benefits formation of perovskite films with good crystallinity. The films spin-coated under low relative humidity (RH) followed by annealing under high RH show an increase of crystallinity and improved performance of devices. Therefore, a mechanism of fast nucleation followed by modest crystal growth (high supersaturation at spin-coating stage and modest supersaturation at annealing stage) is suggested in the formation of high-quality perovskite films.

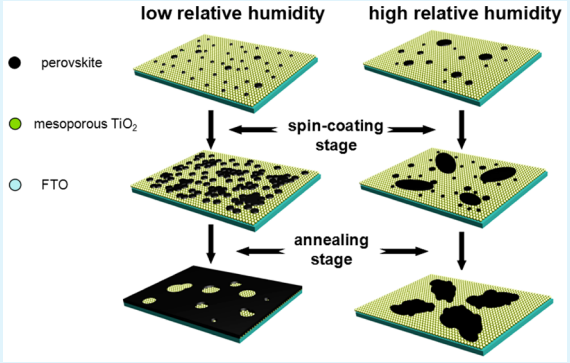

KEYWORDS: *methylammonium lead trihalide, ambient humidity, film coverage, nucleation density, crystal growth*

1. INTRODUCTION

Since the pioneering work of Miyasaka et al. in 2009,[1] organic–inorganic hybrid perovskite solar cells (PSCs) have attracted much attention due to their power conversion efficiencies (PCEs), which improved rapidly from 3.8% to 20.1%.[1−7] As light absorber in PSCs, the hybrid methylammonium lead halide perovskite materials ($CH_3NH_3PbX_3$, X = halogen) combine the advantages of organic compounds and inorganic semiconductors, such as solution processability and tunable optical properties of the organic compounds and ultrahigh light absorption, high charge mobility, and small exciton binding energy of the inorganic semiconductors.[8−10] These advantages make the perovskite materials very promising for application in solar conversion devices.

The solution processability of these perovskite materials is one of the most important advantages. One-step spin-coating method was adopted earlier to deposit perovskite films because of its simple and low-cost process. During the spin-coating and annealing process, solvent evaporation and the following self-assembly induce the formation of crystallized perovskite films. To obtain good performance for PSCs, perovskite films with high quality are necessary. However, the one-step spin-coating method is difficult to yield homogeneous perovskite films; some pinholes appear in the films and degrade the performance of PSCs. The pinholes not only weaken the light absorption ability of perovskite films but also deleteriously impact charge transport and recombination. The coverage of perovskite layer is influenced by many factors, such as the choice of solvent, substrate, spin-coating rate and time, precursor concentration, annealing protocol, and so on. These technology parameters control the nucleation and growth of perovskite films and determine the ultimate crystallinity and morphology. Many endeavors have been tried to improve perovskite morphology and crystallinity by adjusting the above parameters.[4,11,12] Meanwhile, some new preparation methods were developed to improve PCEs of PSCs, such as two-step sequential solution

Received: January 29, 2015
Accepted: April 14, 2015
Published: April 14, 2015

DOI: 10.1021/acsami.5b00895
ACS Appl. Mater. Interfaces 2015, 7, 9110−9117

deposition, vapor deposition, and derivative preparations.[5,13−16] However, the vapor deposition is likely to increase the manufacturing cost. So the solution preparation methods still receive much attention.

In the solution preparation methods, an important factor of ambient humidity has to be faced. It is well-known that the perovskite $CH_3NH_3PbI_3$ films are very sensitive to moisture and the long-term action of moisture could corrode $CH_3NH_3PbI_3$ into PbI_2.[17,18] So the device fabrication should be carried out under controlled atmosphere conditions with low humidity. Many research groups fabricated $CH_3NH_3PbI_3$-based PSCs with high PCEs in a glovebox with RH of <1% or even <1 ppm.[5,19] Meanwhile, some researchers acquired high-performance Cl-doping PSCs in air environment without harsh humidity restriction (RH usually below 30%).[4,20] Despite the ambient humidity during preparation having a significant effect on the photovoltaic performance of PSCs, little has been reported about it. Eperon et al. found that the morphology of samples prepared in a dry glovebox was notably different from the air-processed samples and attributed it to the lack of moisture.[12] Zhou et al. and You et al. reported that postannealing perovskite film in humid air rather than in dry air could improve the performance of the solar cell.[6,21] These phenomena and results seem conflicting and confusing. Moreover, the pivotal role and influence of ambient humidity and moisture during preparation of perovskite films still remain unclear.

In fact, the performance of the solar cell is influenced significantly by both morphology and crystallinity of the film, which are formed through crystallization process of perovskite materials. There is a series of thermodynamic and kinetic steps (deposition of atoms, diffusion, nucleation, and growth) in the crystallization process. These steps may be influenced by moisture differently, and understanding them can help to improve the quality of final films. In this work, we aimed to clarify the role of moisture in perovskite crystallization and to study nucleation and crystal growth of perovskite films under different RH. Different perovskite films were fabricated under four humidity conditions by a conventional one-step spin-coating method. It is found that the coverage of the perovskite films decreases obviously with increasing RH, resulting in higher light transmittance and lower PCEs of PSCs. Further analyses show that for perovskite crystallization the influence of ambient humidity on nucleation at spin-coating stage is different from that on crystal growth at annealing stage. At spin-coating stage, the participation of moisture causes decreased supersaturation and low nucleation density. Most of the morphological differences encountered during preparation of perovskite film can be attributed to the nucleation density. But at the annealing stage, the decreased supersaturation leads to modest crystal growth and benefits the formation of perovskite films with good crystallinity. These insights are important for understanding the perovskite film growth mechanism.

2. EXPERIMENTS

2.1. Materials. All the chemicals were used as received, including titanium diisopropoxide bis(acetylacetonate) (75 wt % in isopropanol, Sigma-Aldrich), 1-butanol (99.8%, Sigma-Aldrich), TiO_2 paste (Dyesol 18NR-T), HI (57% in water, Sigma-Aldrich), CH_3NH_2 (33% in ethanol, Sigma-Aldrich), PbI_2 (99.9983%, Alfa Aesar), $PbCl_2$ (99.99%, Aladdin), *N*,*N*-dimethylformamide (DMF, anhydrous 99.5%, Aladdin), lithium bis(trifluoromethylsulfonyl)imide (Li-TFSI, Sigma-Aldrich), spiro-MeOTAD (99%, Shenzhen Feiming), chlorobenzene (Sigma-Aldrich), acetone, ethanol, acetonitrile. CH_3NH_3I was synthesized in our laboratory as reported by Lee et al.[4]

2.2. mp-TiO_2/c-TiO_2/FTO Substrate Preparation. Initially fluorine-doped tin dioxide (FTO) conductive glass with a sheet resistance of 15 Ω/sq was removed from regions under the anode contact by etching with 2 M HCl and zinc powder. The etched FTO substrates were cleaned by ultrasonic washing in a detergent solution, deionized water, acetone, and ethanol for 20 min in succession, then treated with ultraviolet ozone cleaning for 30 min. A compact TiO_2 (c-TiO_2) layer on the FTO glass was prepared by spin-coating 0.15 M titanium diisopropoxide bis(acetylacetonate) solution in 1-butanol at 3000 rpm for 30 s and drying at 125 °C for 5 min. This was then repeated twice with 0.3 M of titanium diisopropoxide bis(acetylacetonate) solution, and the sample was finally heated at 500 °C for 30 min. After that, TiO_2 paste was diluted by ethanol at 1:3.5 by weight and then deposited on the substrates by spin-coating at 3000 rpm for 30 s. After being dried at 125 °C, the film was annealed at 500 °C for 30 min in air, then immersed in 40 mM aqueous $TiCl_4$ at 70 °C for 30 min to enhance the bonding strength between the oxide films. The thickness of mesoporous TiO_2 (mp-TiO_2) layer is about 300−400 nm (Figure S1a). Then the substrates were transferred and the following deposition processes were conducted in different atmospheres.

2.3. Perovskite Films and Solar Cells Fabrication. *Humidity Control.* The treatments under RH < 1 ppm were processed in a commercial nitrogen-filled glovebox with circulating filtration system (Mikrouna Super). The treatments under RH ≈ 10 ± 5% were processed in a self-built glovebox by controlling nitrogen flow, and the others were processed in air.

Preparation of Perovskite Precursor Solutions. 1:1.2 ratio of PbI_2/CH_3NH_3I and 1:3 ratio of $PbCl_2$/CH_3NH_3I were mixed in DMF under RH < 1 ppm, respectively. The solution (40 wt %) was stirred at room temperature overnight.

Fabrication of Perovskite Films. The perovskite precursor solutions were deposited onto FTO/c-TiO_2/mp-TiO_2 substrates at 60 °C by one-step spin-coating at 2000 rpm for 30 s, followed by annealing on a hot-plate at 100 °C in various atmospheres with RH of <1 ppm, 10 ± 5%, 40 ± 5%, and 70 ± 10%, respectively. The annealing time for $CH_3NH_3PbI_3$ samples was 15 min under all atmospheres due to their fast crystallization, but that for full darkness of $CH_3NH_3PbI_{3-x}Cl_x$ films was different, about 20, 60, 80, and 90 min for RH of <1 ppm, ∼10%, ∼40%, and ∼70% (the time difference between the last two is subtle), respectively.

Fabrication of HTM Layers and Counter Electrodes. After the deposition of perovskite materials, a hole transport material (HTM) solution was coated at 2500 rpm for 30 s. The HTM solution consisted of 72.3 mg of spiro-MeOTAD, 17.5 μL of Li-TFSI in acetonitrile (500 mg/mL), and 28.8 μL of *tert*-butylpyridine (TBP) in 1 mL of chlorobenzene. Finally, thermal evaporation was used to deposit Ag (about 100 nm thickness) for the counter electrodes.

2.4. Characterization. A FEI NOVA NanoSEM230 scanning electron microscopy (SEM) was employed to characterize the morphological properties of all samples. X-ray diffraction (XRD) patterns were collected on a Rigaku Ultima III X-ray diffractometer (Cu Kα) in the range of 10°−60° (2θ). The $J-V$ testing of the PSCs with an active area of 0.24 cm^2 employed a Keithley 2400 source measure unit under AM 1.5 illumination cast by an Oriel 92251A-1000 sunlight simulator. A Shimadzu UV-2550 UV−vis spectrometer fitted with an integrating sphere was used to investigate the optical transmittance spectra of the films. The incident photon-to-current conversion efficiency (IPCE) spectrum was collected with a self-built apparatus. Time-resolved photoluminescence was acquired using the time-correlated single-photon counting technique, and the excitation was provided by a picosecond diode laser at a wavelength of 400 nm with a repetition frequency of 4 MHz.

DOI: 10.1021/acsami.5b00895
ACS Appl. Mater. Interfaces 2015, 7, 9110−9117

Table 1. $CH_3NH_3PbI_3$ and $CH_3NH_3PbI_{3-x}Cl_x$ Samples Fabricated in Different Atmospheres

	samples							
	P-1	P-2	P-3	P-4	P_{cl}-1	P_{cl}-2	P_{cl}-3	P_{cl}-4
precursor	PbI_2 + CH_3NH_3I (1:1.2) in DMF				$PbCl_2$ + CH_3NH_3I (1:3) in DMF			
preparation RH	<1 ppm	10%	40%	70%	<1 ppm	10%	40%	70%

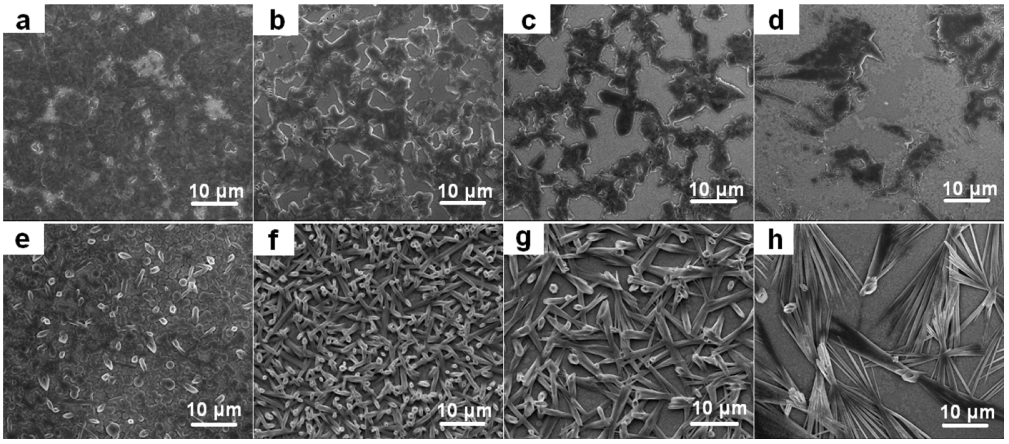

Figure 1. SEM images of perovskite $CH_3NH_3PbI_{3-x}Cl_x$ films (top row) and $CH_3NH_3PbI_3$ films (bottom row) deposited on mp-TiO_2 layer under different ambient humidities: (a) P_{cl}-1; (b) P_{cl}-2; (c) P_{cl}-3; (d) P_{cl}-4; (e) P-1; (f) P-2; (g) P-3; (h) P-4.

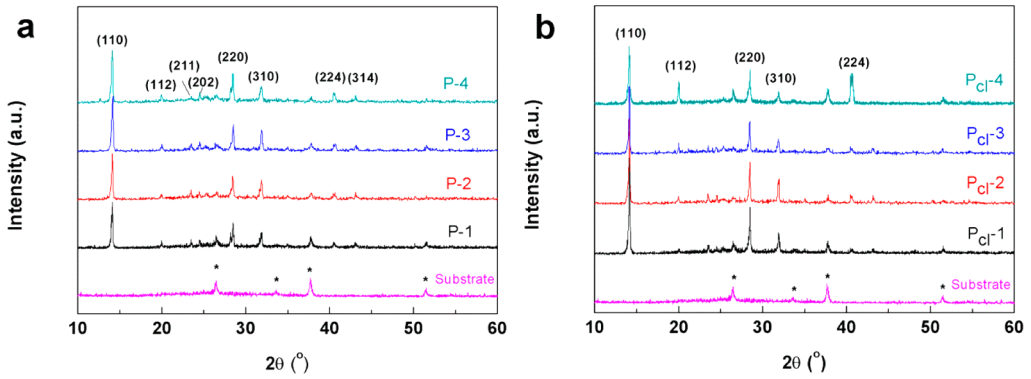

Figure 2. XRD patterns corresponding to perovskite films prepared under different ambient humidities: (a) $CH_3NH_3PbI_3$; (b) $CH_3NH_3PbI_{3-x}Cl_x$. Diffraction peaks for the mp-TiO_2/c-TiO_2/FTO substrate are marked by ⋆.

3. RESULTS AND DISCUSSION

Nowadays the most commonly studied perovskites are $CH_3NH_3PbI_3$ and $CH_3NH_3PbI_{3-x}Cl_x$. In order to ensure good repeatability and reproducibility of experimental results, we changed the ambient humidity and kept the other parameters unchanged unless especially mentioned. The $CH_3NH_3PbI_3$ and $CH_3NH_3PbI_{3-x}Cl_x$ samples fabricated in different atmospheres are denoted in Table 1 to facilitate understanding. It is worth mentioning that the recent argument over the residual Cl in the final $CH_3NH_3PbI_{3-x}Cl_x$ films has shown no measurable quantity of Cl after annealing.[20,22,23] The discussion of remaining Cl is beyond the scope of this study. Therefore, we still adopt $CH_3NH_3PbI_{3-x}Cl_x$ to denote the Cl-doping perovskite system for convenience and clarity.

The influence of ambient humidity on the surface morphology of perovskite layer on mp-TiO_2 layer was examined by scanning electron microscopy (SEM), and the morphological characterization of mp-TiO_2 layer is shown in Figure S1b in Supporting Information. As reported previously, $CH_3NH_3PbI_{3-x}Cl_x$ crystals are formed on top of the mesoporous film and the coverage of the perovskite layer is not complete for all the samples.[11,12,24,25] Moreover, the exposed surface of mp-TiO_2 layer increases obviously with RH. For samples prepared under RH less than 1 ppm, the coverage of $CH_3NH_3PbI_{3-x}Cl_x$ film is highest and the shape of the crystallites is much planar (Figure 1a). As the RH is increased to ∼10%, there is a big change in the appearance of the formed film. The microparticles in connection with each other are observed and cover less surface of the substrate (Figure 1b). The film formed under RH ≈ 40% is relatively similar in appearance to that formed under RH ≈ 10%, but the perovskite crystallites are no longer attached densely to each other and the spacing between them are larger (Figure 1c). So the coverage of perovskite layer is further reduced. With an increase of RH to 70%, the formed perovskite crystallites adopts a larger individual size for islands (Figure 1d). These island-shape crystallites have large sizes of dozens of micrometers and larger spacing in between, resulting in the largest uncovered mp-TiO_2 surface among these four cases.

Similar changes also happened in $CH_3NH_3PbI_3$ films. In the bottom row of Figure 1, the $CH_3NH_3PbI_3$ films deposited by conventional spin-coating contain rod-shape crystals, which is

DOI: 10.1021/acsami.5b00895
ACS Appl. Mater. Interfaces 2015, 7, 9110−9117

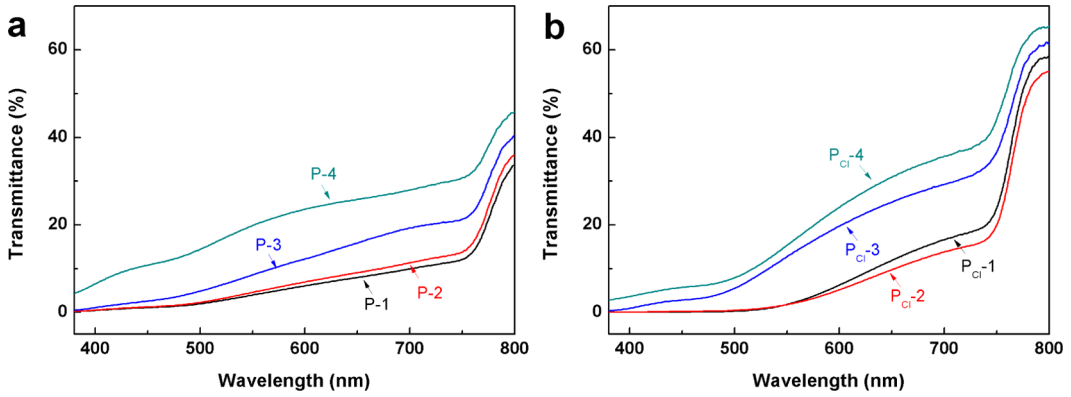

Figure 3. Transmittance spectra of (a) $CH_3NH_3PbI_3$ films and (b) $CH_3NH_3PbI_{3-x}Cl_x$ films deposited on mp-TiO_2 film under different RH.

in accordance with previous observation.[5,26] Compared to the $CH_3NH_3PbI_{3-x}Cl_x$ film, the rod-shape morphology leads to poorer surface coverage. But the rod-shape crystal size and exposed substrate areas increase with the RH, same as the $CH_3NH_3PbI_{3-x}Cl_x$ film. Figure 1 indicates that the morphology of perovskite films is significantly influenced by the ambient humidity, and high RH always results in large crystal islands of perovskites and the associated large spacing in between, leading to low surface coverage.

Figure 2 compares the X-ray diffraction (XRD) patterns of $CH_3NH_3PbI_3$ and $CH_3NH_3PbI_{3-x}Cl_x$ films prepared under different ambient humidities. It is worth noting that it takes different time to make $CH_3NH_3PbI_{3-x}Cl_x$ films fully darkened under different ambient humidities while the annealing temperature is fixed at 100 °C. This process will be discussed below in detail. The X-ray diffractograms of $CH_3NH_3PbI_{3-x}Cl_x$ films are similar to that of $CH_3NH_3PbI_3$ films because there is no measurable quantity of Cl after annealing,[20,22] and both are in agreement with spectra previously reported for these materials in the literature.[26] $CH_3NH_3PbI_3$ is a type of polar tetragonal material at room temperature, and the $CH_3NH_3PbI_3$ films usually demonstrate the preferred orientation of (110) peak.[27] Intense diffraction peaks at 14.08°, 20.48°, 28.40°, 31.86°, and 43.19° can be assigned to (110), (112), (220), (310), and (224) diffractions, respectively. Figure 2a indicates that without any change in pattern positions, the intense diffraction peaks of $CH_3NH_3PbI_3$ samples seem to be slightly stronger with increasing RH. For $CH_3NH_3PbI_{3-x}Cl_x$ samples, the (112) and (224) diffraction peaks become obviously stronger under the highest humidity investigated (RH ≈ 70%), suggesting a possible change of the grain crystal orientation and granulation of perovskite film. These results imply that during preparation process the brief action of moisture may not result in the destruction of perovskite crystallization but a change of grain sizes and preferential orientation.

The transmittance spectra of the perovskite films prepared under different ambient humidities were also measured, and the results are shown in Figure 3. As reported, the perovskite layers deposited on mp-TiO_2 demonstrate a panchromatic absorption of light with spectra that extend over the visible to near-infrared region.[4,5] The difference in ambient humidity has an obvious influence on the light transmittance of the as-prepared films for both $CH_3NH_3PbI_3$ and $CH_3NH_3PbI_{3-x}Cl_x$, which generally increases with RH. Two factors may be responsible for the transmittance: film thickness and coverage. For the same amount of starting material, the final film volume should be the same; hence, the regions of perovskite in film with less coverage are thicker. Compared to the condition of RH < 1 ppm, the film coverage prepared under RH ≈ 10% decreases slightly with increased film thickness, so the difference in transmittance is subtle. With an increase of the ambient humidity to RH ≈ 40% or RH ≈ 70%, the worse coverage leads to plenty of light transmittance from the uncovered regions. The low coverage induced by high ambient humidity results in high transmittance and poor absorption of light.

To determine the effect of ambient humidity on the photovoltaic properties of PSCs, we fabricated cells with the corresponding perovskite films. The annealing temperature and time largely influence the crystallization of perovskite materials; too short or too long annealing time lead to insufficient crystallization or decomposition of them, respectively.[11] Therefore, the performance of PSCs based on properly crystallized perovskite films was compared. Typical current density−voltage (J−V) curves under AM 1.5 (100 mW cm^{-2}) illumination with an active area of 0.24 cm^2 are presented in parts a and b of Figure 4. A clear correlation is observed between the coverage of perovskite films and the photovoltaic performance of the cells. The short-circuit photocurrent (J_{sc}), open-circuit voltage (V_{oc}), and PCEs decrease in different degrees with the coverage rate. Compared to absolute $CH_3NH_3PbI_3$, the performance of Cl-doping PSCs has obviously less dependence on RH, which is in accordance with reported cases.[4,6,20] Mean device PCEs for a single batch of PSCs prepared under different humidity conditions are also shown in Figure 4c. High light transmittance is the main reason for decreasing J_{sc}, and the reductive V_{oc} could be attributed to the reduced carrier lifetime resulting from pinholes.[11,12,19] We also used time-resolved photoluminescence (PL) to characterize the carrier recombination in perovskite films, as shown in Figure S2. The PL lifetimes of both $CH_3NH_3PbI_3$ and $CH_3NH_3PbI_{3-x}Cl_x$ films have been prolonged significantly as a result of the homogeneous absorber layer with fewer pinholes.

To investigate the reasons for the differences between these perovskite films prepared under different ambient humidities, we must try to understand their crystallization process. The crystallization of thin film is a very complicated process and is of importance in many fields. It includes a series of thermodynamic and kinetic steps, which are deposition of atoms, diffusion, nucleation, and growth.[28−30] So far for solution-processed perovskite cells, the perovskite layer is typically prepared by the chemical solution coating method. As the solvent evaporated, the precursor solution attains supersaturation status and precipitates atoms. The atoms diffuse on the substrate because of thermal motion and concentration

DOI: 10.1021/acsami.5b00895
ACS Appl. Mater. Interfaces 2015, 7, 9110−9117

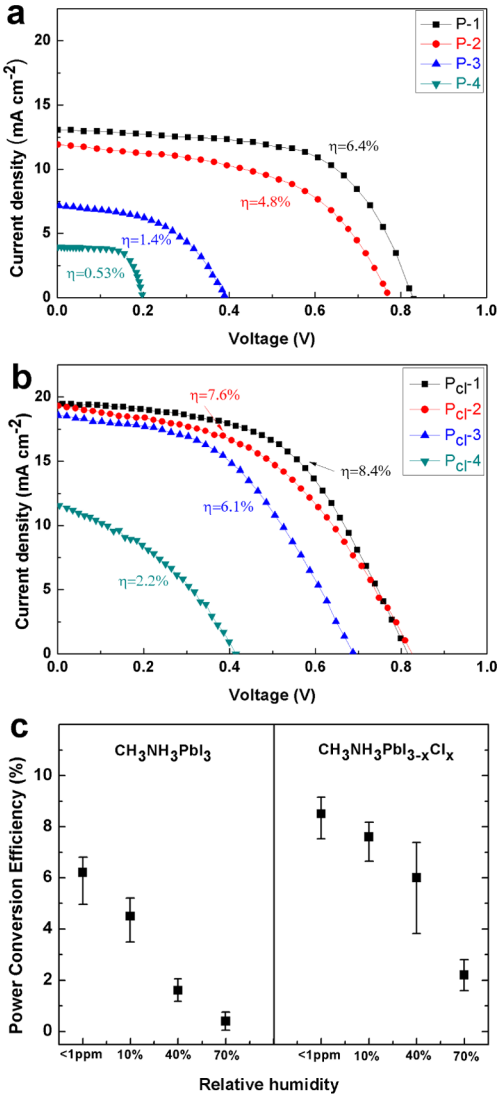

Figure 4. $J-V$ curves of the perovskite solar cells prepared under different ambient humidities: (a) $CH_3NH_3PbI_3$; (b) $CH_3NH_3PbI_{3-x}Cl_x$. (c) Dependence of the PCEs on RH. Each data point represents the mean from a set of 10 devices.

gradient, further combining with each other to lower their Gibbs free energy (called self-assembly). Then a number of nucleation sites appear on the substrate and capture more atoms to produce crystals with stability. According to thin film growth theory, the film growth process usually expresses three types: layer growth (Frank–van der Merwe), island growth (Volmer–Weber), and Stranski–Krastanov growth.[31] The growth type depends on interface free energy G and supersaturation ξ. In chemical solution coating method, the nucleation and growth of crystal are driven by the supersaturation, which is usually defined with the following equation:[31]

$$\xi = \frac{\rho_s - \rho_e}{\rho_e} = \frac{\rho_s}{\rho_e} - 1$$

in which ρ_s is the concentration of supersaturation and ρ_e is the concentration of equilibrium status. Increased supersaturation is conducive to small critical nucleus radius and high nucleation density[32] and is better for layer growth. For example, high supersaturation induced by fast solvent evaporation usually leads to fast nucleation and high nucleation density.[26,33,34] Figure S3a and correlative formulas show the relationship between supersaturation and critical nucleus, crystal growth mode.

It is well-known that the organic species in the $CH_3NH_3PbX_3$ phases are hygroscopic.[17,18] At the spin-coating stage, with evaporation of DMF the perovskite precursor solutions attain equilibrium and supersaturation status in sequence, then begin to nucleate. But under humid circumstance, the films could absorb moisture. The adsorption of water would increase the amount of residual solvent and delay supersaturation status of solution, resulting in decreased ρ_s and ξ (Figure 5).[35]

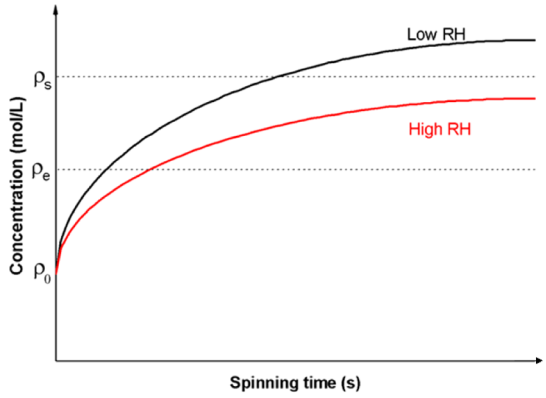

Figure 5. Schematic illustration for nucleation during spin-coating: the relation between solution concentration and spinning time. ρ_0 is concentration of precursor solution. ρ_e is concentration of equilibrium status, and ρ_s is concentration of supersaturation.

According to thin film growth theory, low ξ usually leads to large critical nucleus radius, low nucleation density, and island growth of perovskite film. Therefore, we compared the SEM images of $CH_3NH_3PbI_{3-x}Cl_x$ films prepared under RH ≈ 10% and RH ≈ 70% at different times of annealing. The effect of the solution deposition is separated from those of the thermal treatment in Figure 6a and Figure 6e because the annealing time of samples is 0 min. It is found that the difference of the film morphology is determined before the annealing stage. Just after spin-coating, solvent evaporation resulted in the formation of many small and dense crystals scattered uniformly on mp-TiO_2 substrates under RH ≈ 10%. The further annealing made

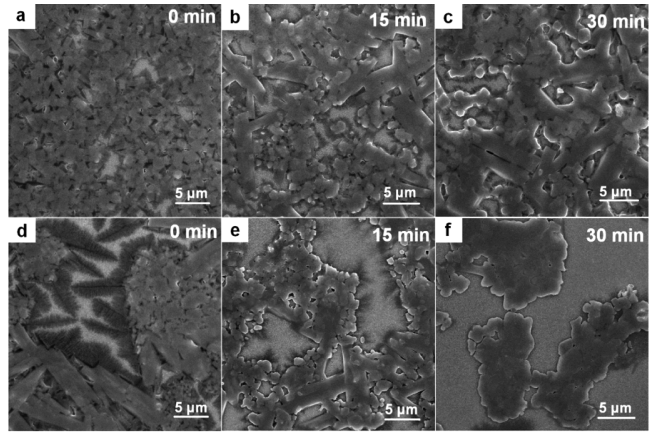

Figure 6. SEM images of $CH_3NH_3PbI_{3-x}Cl_x$ films annealed at 100 °C under (a–c) RH ≈ 10% and (d–f) RH ≈ 70% for different times.

DOI: 10.1021/acsami.5b00895
ACS Appl. Mater. Interfaces 2015, 7, 9110–9117

more solvent evaporated and these crystals grown, fused, and interconnected to each other to form a film with considerable coverage as shown in Figure 6b and Figure 6c. But under the condition of RH ≈ 70%, where large crystals and aggregations were formed as in Figure 6d, there was no nucleation site on some areas of substrate, resulting in the formation of pinholes in the final films. It is revealed that at the spin-coating stage the nucleation density of perovskite prepared under high humidity is less than that prepared under low humidity and directly determines the ultimate morphology of perovskite films. Compared to Cl-doping of perovskite films, we also note that absolute $CH_3NH_3PbI_3$ films prepared by one-step spin-coating method are more sensitive to ambient humidity.[4,15,19,20] The phenomenon further confirms our analysis because the $PbCl_2$ nanocrystals added to the $CH_3NH_3PbI_{3-x}Cl_x$ precursor solution can partly play the role of nucleation sites.[33] So at the spin-coating stage, increased supersaturation and high nucleation density can help contribute to homogeneous morphology of the final perovskite films.

As a driving force of the crystallization process, supersaturation has a major effect on the growth rate because by definition it is connected with the difference of the chemical potentials $\Delta\mu$ of the solution and crystal.[36,37] Crystals grow slowly at low supersaturation. And high supersaturation causes fast crystal growth, resulting in spontaneous nucleation from the solution and formation of defects in the crystals. These disadvantages are not induced by supersaturation itself but the difference of supersaturation in different crystal planes.[31,38] The higher the supersaturation is, the bigger the difference of supersaturation is. In an ideal case, the perfect crystal grows layer by layer. However, the difference of supersaturation in different crystal planes rules out this possibility. Before the former layer is completed, there is always a new layer of atoms grown in the regions with high supersaturation, resulting in destruction of crystal structure and a large number of defects (as shown in Figure S3b). Therefore, a modest supersaturation is better for perovskite crystal growth. It was observed that at the annealing stage the adsorption of water could slow the crystallization of perovskite films. Figure 7 shows the effect of

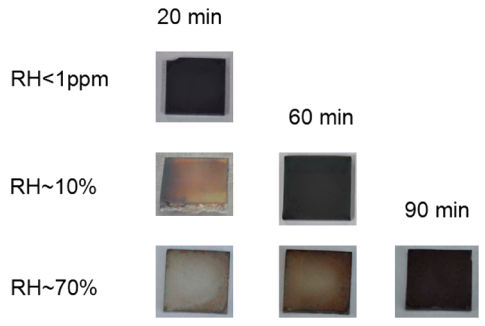

Figure 7. Images of the $CH_3NH_3PbI_{3-x}Cl_x$ films prepared under different ambient humidities and annealed at 100 °C with varying duration (as indicated).

varying annealing time at 100 °C on the appearance of perovskite $CH_3NH_3PbI_{3-x}Cl_x$ films prepared under different ambient humidities. Just after spin-coating, all perovskite precursor films were yellowish. When prepared under the condition of RH < 1 ppm, the perovskite film turned dark brown within about 20 min. With increasing humidity to RH ≈ 10%, the annealing process that turned the perovskite film dark brown occurred at significantly slower rates; it took about 60 min for the perovskite film to turn dark brown. When under the higher ambient humidities investigated (RH ≈ 40% and RH ≈ 70%), the full darkness of the perovskite material needs a longer time of about 80−90 min (the difference between the two is subtle). Considering of the XRD data results, the adsorption of water slows the darkening process of perovskite films, which is correlated to their crystallization. We speculate that the same goes for $CH_3NH_3PbI_3$ films, but it is difficult to distinguish directly because of their relative fast crystallization. It is worth noting that the precursor solution used here was fresh.

It has been reported that nonannealed perovskite films degraded rapidly in moist atmosphere.[12] But our SEM and XRD analyses indicate that the perovskite films annealed under high ambient humidity are still able to crystallize, only with a low speed. A nonequilibrium chemical reaction may be involved in this slow crystallization of perovskite films. The self-assembly driven by thermal motion promotes the crystallization of these perovskite materials (reaction 1),[11,22] but $CH_3NH_3PbI_3$ is easily decomposed by the action of moisture (reaction 2).[18]

$$PbCl_2(s) + 3CH_3NH_3I(aq) \xrightarrow{\text{self-assembly}} CH_3NH_3PbI_3(s) + 2CH_3NH_3Cl(g) \quad (1)$$

$$CH_3NH_3PbI_3(s) \underset{\text{self-assembly}}{\overset{\text{moisture}}{\rightleftharpoons}} PbI_2(s) + CH_3NH_3I(aq) \quad (2)$$

At the same temperature, the chemical equilibrium of this reaction may be regulated by the moisture. Annealing at 100 °C accelerates the self-assembly and evaporates the absorbed water, so the crystallization of perovskites can still go on under humid conditions but with a slow rate.

To further verify our analysis, $CH_3NH_3PbI_{3-x}Cl_x$ films have been spin-coated under RH ≈ 10% and annealed in air with RH ≈ 70%. Compared to the sample thoroughly prepared under RH ≈ 10%, this sample with an improved PCE of 10.1% has more flat surface morphology (Figure S4) and shows an increase of crystallinity and preferred orientation of perovskite (Figure 8), which are consistent with the former analysis. The IPCE of the optimized devices is shown in Figure S4b. The peak value of IPCE has reached up to 79.8%, and the integrated J_{sc} is 18.7 mA/cm^2, which is in good accordance with the measured J_{sc} (19.5 mA/cm^2) of the $J-V$ curves. We also investigated the reproducibility of these optimized devices. The photovoltaic parameters of a batch of ten devices are shown in Table S1; the average V_{oc}, J_{sc}, FF, and PCE are 0.88 ± 0.02 V, 19.1 ± 0.6 mA/cm^2, 0.58 ± 0.03, and 9.9 ± 0.5%, respectively. Therefore, fast nucleation can improve the coverage of films, and modest crystal growth can contribute to good crystallinity. So a mechanism of fast nucleation followed by modest crystal growth (high supersaturation at spin-coating stage and modest supersaturation at annealing stage) is suggested in the formation of high-quality perovskite films.

4. CONCLUSION

In summary, we investigated the effect of ambient humidity on surface morphology and crystallinity of perovskite films and the performance of perovskite solar cells. Our work demonstrates that the coverage of perovskite layer decreases obviously with increasing RH, resulting in higher light transmittance and lower PCEs of perovskite cells. By examining the effect of different annealing times in the crystallization process, we conclude that

DOI: 10.1021/acsami.5b00895
ACS Appl. Mater. Interfaces 2015, 7, 9110−9117

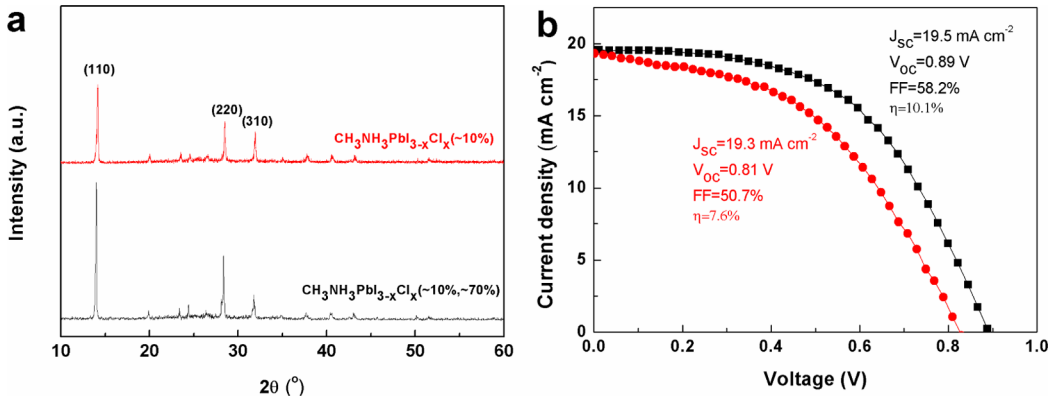

Figure 8. Comparisons of (a) XRD patterns and (b) *J*–*V* curves between $CH_3NH_3PbI_{3-x}Cl_x$ film thoroughly prepared under RH ≈ 10% (red) and $CH_3NH_3PbI_{3-x}Cl_x$ film spin-coated under RH ≈ 10% followed by annealing under RH ≈ 70% (black).

the supersaturation and nucleation density play key roles in the crystallization of these materials. The low nucleation density induced by decreased supersaturation appears under high humid conditions and causes island growth of perovskite films. But at the annealing stage, the modest crystal growth under high humid conditions can benefit the formation of perovskite films, such as better crystallinity and lower crystal defect density. In this way, the $CH_3NH_3PbI_{3-x}Cl_x$ films which were spin-coated under low RH followed by annealing under high RH show an increase of crystallinity and improved performance of PSCs. These insights into the perovskite crystallization affected by moisture may aid in further improvement and understanding of the devices.

■ ASSOCIATED CONTENT

Supporting Information

SEM cross-sectional image; time-resolved PL decay curves; discussion on the critical nucleus size; photovoltaic parameters of a batch of 10 devices based on $CH_3NH_3PbI_{3-x}Cl_x$ films spin-coated under RH ≈ 10% followed by annealing under RH ≈ 70%; IPCE of corresponding device. These materials are available free of charge via the Internet at http://pubs.acs.org.

■ AUTHOR INFORMATION

Corresponding Author

*E-mail: yutao@nju.edu.cn.

Notes

The authors declare no competing financial interest.

■ ACKNOWLEDGMENTS

This work was supported primarily by the National Natural Science Foundation of China (Grants 11174129 and 61377051), the National Basic Research Program of China (Grants 2011CB933303 and 2013CB632404), the Science and Technology Research Program of Jiangsu Province (Grant BK20130053), and the College Postgraduate Research and Innovation Project of Jiangsu Province (Grant KYZZ_0025). We thank Prof. Chunfeng Zhang and Dr. Qi Chen for their help with the time-resolved PL decay experiments.

■ REFERENCES

(1) Kojima, A.; Teshima, K.; Shirai, Y.; Miyasaka, T. Organometal Halide Perovskites as Visible-Light Sensitizers for Photovoltaic Cells. *J. Am. Chem. Soc.* **2009**, *131*, 6050–6051.

(2) Im, J. H.; Lee, C. R.; Lee, J. W.; Park, S. W.; Park, N. G. 6.5% Efficient Perovskite Quantum-Dot-Sensitized Solar Cell. *Nanoscale* **2011**, *3*, 4088–4093.

(3) Kim, H. S.; Lee, C. R.; Im, J. H.; Lee, K. B.; Moehl, T.; Marchioro, A.; Moon, S. J.; Humphry-Baker, R.; Yum, J. H.; Moser, J. E.; Grätzel, M.; Park, N. G. Lead Iodide Perovskite Sensitized All-Solid-State Submicron Thin Film Mesoscopic Solar Cell with Efficiency Exceeding 9%. *Sci. Rep.* **2012**, *2*, 591:1–7.

(4) Lee, M. M.; Teuscher, J.; Miyasaka, T.; Murakami, T. N.; Snaith, H. J. Efficient Hybrid Solar Cells Based on Meso-Superstructured Organometal Halide Perovskites. *Science* **2012**, *338*, 643–647.

(5) Burschka, J.; Pellet, N.; Moon, S. J.; Humphry-Baker, R.; Gao, P.; Nazeeruddin, M. K.; Grätzel, M. Sequential Deposition as a Route to High-Performance Perovskite-Sensitized Solar Cells. *Nature* **2013**, *499*, 316–319.

(6) Zhou, H. P.; Chen, Q.; Li, G.; Luo, S.; Song, T. B.; Duan, H. S.; Hong, Z. R.; You, J. B.; Liu, Y. S.; Yang, Y. Interface Engineering of Highly Efficient Perovskite Solar Cells. *Science* **2014**, *345*, 542–546.

(7) Jeon, N. J.; Noh, J. H.; Yang, W. S.; Kim, Y. C.; Ryu, S.; Seo, J.; Seok, S. I. Compositional Engineering of Perovskite Materials for High-Performance Solar Cells. *Nature* **2015**, *517*, 476–480.

(8) Ponseca, C. S.; Savenije, T. J.; Abdellah, M.; Zheng, K.; Yartsev, A.; Pascher, T.; Harlang, T.; Chabera, P.; Pullerits, T.; Stepanov, A.; Wolf, J. P.; Sundstrm, V. Organometal Halide Perovskite Solar Cell Materials Rationalized: Ultrafast Charge Generation, High and Microsecond-Long Balanced Mobilities and Slow Recombination. *J. Am. Chem. Soc.* **2014**, *136*, 5189–5192.

(9) Yin, W. J.; Shi, T. T.; Yan, Y. F. Unique Properties of Halide Perovskites as Possible Origins of the Superior Solar Cell Performance. *Adv. Mater.* **2014**, *26*, 4653–4658.

(10) Wehrenfenning, C.; Eperon, G. E.; Johnston, M. B.; Snaith, H. J.; Herz, L. M. High Charge Carrier Mobilities and Lifetimes in Organolead Trihalide Perovskites. *Adv. Mater.* **2014**, *26*, 1584–1589.

(11) Dualeh, A.; Tétreault, N.; Moehl, T.; Gao, P.; Nazeeruddin, M. K.; Grätzel, M. Effect of Annealing Temperature on Film Morphology of Organic-Inorganic Hybrid Pervoskite Solid-State Solar Cells. *Adv. Funct. Mater.* **2014**, *24*, 3250–3258.

(12) Eperson, G. E.; Burlakov, V. M.; Docampo, P.; Goriely, A.; Snaith, H. J. Morphological Control for High Performance, Solution-Processed Planar Heterojunction Perovskite Solar Cells. *Adv. Funct. Mater.* **2014**, *24*, 151–157.

(13) Liu, M. Z.; Johnston, M. B.; Snaith, H. J. Efficient Planar Heterojunction Perovskite Solar Cells by Vapour Deposition. *Nature* **2013**, *501*, 395–398.

(14) Chen, Q.; Zhou, H. P.; Hong, Z. R.; Luo, S.; Duan, H.-S.; Wang, H.-H.; Liu, Y. S.; Li, G.; Yang, Y. Planar Heterojunction Perovskite Solar Cells via Vapor Assisted Solution Process. *J. Am. Chem. Soc.* **2014**, *136*, 622–625.

(15) Shi, J. J.; Luo, Y. H.; Wei, H. Y.; Luo, J. H.; Dong, J.; Lv, S. T.; Xiao, J. Y.; Xu, Y. Z.; Zhu, L. F.; Xu, X.; Wu, H. J.; Li, D. M.; Meng, Q.

DOI: 10.1021/acsami.5b00895
ACS Appl. Mater. Interfaces 2015, 7, 9110–9117

B. Modified Two-Step Deposition Method for High-Efficiency TiO_2/$CH_3NH_3PbI_3$ Heterojunction Solar Cells. *ACS Appl. Mater. Interfaces* **2014**, *6*, 9711−9718.
(16) Wu, Y. Z.; Islam, A.; Yang, X. D.; Qin, C. J.; Liu, J.; Zhang, K.; Peng, W. Q.; Han, L. Y. Retarding the Crystallization of PbI_2 for Highly Reproducible Planar-Structured Perovskite Solar Cells via Sequential Deposition. *Energy Environ. Sci.* **2014**, *7*, 2934−2938.
(17) Grätzel, M. The Light and Shade of Perovskite Solar Cells. *Nat. Mater.* **2014**, *13*, 838−842.
(18) Niu, G. D.; Li, W. Z.; Meng, F. Q.; Wang, L. D.; Dong, H. P.; Qiu, Y. Study on the Stability of $CH_3NH_3PbI_3$ Films and the Effect of Post-Modification by Aluminum Oxide in All-Solid-State Hybrid Solar Cells. *J. Mater. Chem. A* **2014**, *2*, 705−710.
(19) Liang, P. W.; Liao, C.-Y.; Chueh, C.-C.; Zuo, F.; Williams, S. T.; Xin, X. K.; Lin, J. J.; Jen, A. K.-Y. Additive Enhanced Crystallization of Solution-Processed Perovskite for Highly Efficient Planar-Heterojunction Solar Cells. *Adv. Mater.* **2014**, *26*, 3748−3754.
(20) Zhao, Y. X.; Zhu, K. CH_3NH_3Cl-Assisted One-Step Solution Growth of $CH_3NH_3PbI_3$: Structure, Charge-Carrier Dynamics, and Photovoltaic Properties of Perovskite Solar Cells. *J. Phys. Chem. C* **2014**, *118*, 9412−9418.
(21) You, J. B.; Yang, Y. (M.; Hong, Z. R.; Song, T.-B.; Meng, L.; Liu, Y. S.; Jiang, C. Y.; Zhou, H. P.; Chang, W.-H.; Li, G.; Yang, Y. Moisture Assisted Perovskite Film Growth for High Performance Solar Cells. *Appl. Phys. Lett.* **2014**, *105*, 183902.
(22) Yu, H.; Wang, F.; Xie, F. Y.; Li, W. W.; Chen, J.; Zhao, N. The Role of Chlorine in the Formation Process of "$CH_3NH_3PbI_{3-x}Cl_x$" Perovskite. *Adv. Funct. Mater.* **2014**, *24*, 7102−7108.
(23) Williams, S. T.; Zuo, F.; Chueh, C.-C.; Liao, C.-Y.; Liang, P.-W.; Jen, A. K.-Y. Role of Chloride in the Morphological Evolution of Organo-Lead Halide Perovskite Thin Films. *ACS Nano* **2014**, *8*, 10640−10654.
(24) Jeng, J. Y.; Chiang, Y. F.; Lee, M. H.; Peng, S. R.; Guo, T. F.; Chen, P.; Wen, T. C. $CH_3NH_3PbI_3$ Perovskite/Fullerene Planar-Heterojunction Hybrid Solar Cells. *Adv. Mater.* **2013**, *25*, 3727−3732.
(25) Docampo, P.; Ball, J. M.; Darwich, M.; Eperon, G. E.; Snaith, H. J. Efficient Organometal Trihalide Perovskite Planar-Heterojunction Solar Cells on Flexible Polymer Substrates. *Nat. Commun.* **2013**, *4*, 2761.
(26) Xiao, M. D.; Huang, F. Z.; Huang, W. C.; Dkhissi, Y.; Zhu, Y.; Etheridge, J.; Gray-Weale, A.; Bach, U.; Cheng, Y. B.; Spiccia, L. A Fast Deposition-Crystallization Procedure for Highly Efficient Lead Iodide Perovskite Thin-Film Solar Cells. *Angew. Chem.* **2014**, *53*, 9898−9903.
(27) Baikie, T.; Fang, Y.; Kadro, J. M.; Schreyer, M.; Wei, F.; Mhaisalkar, S. G.; Grätzel, M.; White, T. J. Synthesis and Crystal Chemistry of the Hybrid Perovskite $(CH_3NH_3)PbI_3$ for Solid-State Sensitised Solar Cell Applications. *J. Mater. Chem. A* **2013**, *1*, 5628−5641.
(28) Venables, J. A. Nucleation and Growth of Thin-Films. *Rep. Prog. Phys.* **1984**, *47*, 399−459.
(29) Venables, J. A. Rate Equation Approaches to Thin-Film Nucleation Kinetics. *Philos. Mag.* **1973**, *27*, 697−738.
(30) Desiraju; Gautam, R. Crystal Engineering: A Brief Overview. *J. Chem. Sci.* **2010**, *122*, 667−675.
(31) Venables, J. A. *Introduction to Surface and Thin Film Processes*; World Publishing Corporation: Beijing, 2003.
(32) Mukhopadhyay, M.; Dalvi, S. V. Analysis of Supersaturation and Nucleation in a Moving Solution Droplet with Flowing Supercritical Carbon Dioxide. *J. Chem. Technol. Biotechnol.* **2005**, *80*, 445−454.
(33) Tidhar, Y.; Edri, E.; Weissman, H.; Zohar, D.; Hodes, G.; Cahen, D.; Rybtchinski, B.; Kirmayer, S. Crystallization of Methyl Ammonium Lead Halide Perovskites: Implications for Photovoltaic Applications. *J. Am. Chem. Soc.* **2014**, *136*, 13249−13256.
(34) Huang, F. Z.; Dkhissi, Y.; Huang, W. C.; Xiao, M. D.; Benesperi, L.; Rubanov, S.; Zhu, Y.; Lin, X. F.; Jiang, L. C.; Zhou, Y. C.; Gray-Weale, A.; Etheridge, J.; Mcneill, C. R.; Caruso, R. A.; Bach, U.; Spiccia, L.; Cheng, Y. B. Gas-Assisted Preparation of Lead Iodide Perovskite Films Consisting of a Monolayer of Single Crystalline Grains for High Efficiency Planar Solar Cells. *Nano Energy* **2014**, *10*, 10−18.
(35) Heo, J. H.; Song, D. H.; Im, S. H. Planar $CH_3NH_3PbBr_3$ Hybrid Solar Cells with 10.4% Power Conversion Efficiency, Fabricated by Controlled Crystallization in the Spin-Coating Process. *Adv. Mater.* **2014**, *26*, 8179−8183.
(36) Sangwal, K. Growth Kinetics and Surface Morphology of Crystals Growth from Solutions: Recent Observations and Their Interpretations. *Prog. Cryst. Growth Charact. Mater.* **1998**, *36*, 163−248.
(37) Zaitseva, N.; Carman, L. Rapid Growth of KDP-type Crystals. *Prog. Cryst. Growth Charact. Mater.* **2001**, *43*, 1−118.
(38) Zhang, K. C.; Zhang, L. H. *Crystal Growth* (in Chinese); Science Press: Beijing, 1981.

DOI: 10.1021/acsami.5b00895
ACS Appl. Mater. Interfaces 2015, 7, 9110−9117